JOURNAL OF INFORMATION AND COMMUNICATION TECHNOLOGY
http://e-journal.uum.edu.my/index.php/jict

How to cite this article:
Jamaludin, S., Mohamad Ayob, A. F., Mohd Norzeli, S., & Mohamed, S. B. (2022). Adaptive initial contour and partly-normalization algorithm for iris segmentation of blurry iris images. *Journal of Information and Communication Technology, 21*(3), 411-435. https://doi.org/10.32890/jict2022.21.3.5

Adaptive Initial Contour and Partly-Normalization Algorithm for Iris Segmentation of Blurry Iris Images

*[1]Shahrizan Jamaludin, [2]Ahmad Faisal Mohamad Ayob,
[3]Syamimi Mohd Norzeli & [4]Saiful Bahri Mohamed
[1&2]Faculty of Ocean Engineering Technology and Informatics,
Universiti Malaysia Terengganu, Malaysia
[3&4]Faculty of Innovative Design and Technology,
Universiti Sultan Zainal Abidin, Malaysia

*shahrizanj@umt.edu.my
ahmad.faisal@umt.edu.my
syamiminorzeli@unisza.edu.my
saifulbahri@unisza.edu.my
*Corresponding author

Received: 10/2/2022 Revised: 4/4/2022 Accepted: 19/4/2022 Published: 17/7/2022

ABSTRACT

Iris segmentation is a process to isolate the accurate iris region from the eye image for iris recognition. Iris segmentation on non-ideal and noisy iris images is accurate with active contour. Nevertheless, it is currently unclear on how active contour responds to blurry iris images or motion blur, which presents a significant obstacle in iris segmentation. Investigation on blurry iris images, especially on the initial contour position, is rarely published and must be clarified.

Moreover, evolution or convergence speed remains a significant challenge for active contour as it segments the precise iris boundary. Therefore, this study carried out experiments to achieve an efficient iris segmentation algorithm in terms of accuracy and fast execution, according to the aforementioned concerns. In addition, initial contour was explored to clarify its position. In order to accomplish these goals, the Wiener filter and morphological closing were used for pre-processing and reflection removal. Next, the adaptive initial contour (AIC), δ, and stopping function were integrated to create the adaptive Chan-Vese active contour (ACVAC) algorithm. Finally, the partly-normalization method for normalization and feature extraction was designed by selecting the most prominent iris features. The findings revealed that the algorithm outperformed the other active contour-based approaches in computational time and segmentation accuracy. It proved that in blurry iris images, the accurate initial contour position could be established. This algorithm is significant to solve inaccurate segmentation on blurry iris images.

Keywords: Iris segmentation, adaptive initial contour, adaptive Chan-Vese active contour, partly-normalization, segmentation accuracy.

INTRODUCTION

Biometric system sales have been steadily increasing to suit worldwide market demands. In comparison to the traditional system, the biometric system is chosen since it is non-transferable (Sarier, 2021), fraud-resistant (Shrivastava & Tcheslavski, 2018), and very convenient (Hossain et al., 2021). Biometric systems, both contact and contactless, can create adequate identification (Anne et al., 2020) and verification (Blasco & Peris-Lopez, 2018). Contact biometrics, such as fingerprints, are user-friendly (Amreen et al., 2020) and have high accuracy (Alsmirat et al., 2019). Furthermore, the demand for contactless biometric systems during the COVID-19 pandemic is expected to increase. Iris recognition can be utilized from a distance, help maintain personal hygiene, and minimize virus infection (Zhang et al., 2019). Moreover, iris recognition offers many benefits, including the fact that it is difficult to forge (Cohen et al., 2021), spoof-proof (Kaur, 2020), naturally protected from harsh environments (Sujatha & Chilambuchelvan, 2018), gives accurate matching (Wang & Kumar, 2019), and offers high scalability (Shin et al., 2017). This system

contains a massive iris database that can be obtained and accessed through numerous government entities (Chen et al., 2020).

Iris is an annular object in the human eye. It leads the light into the retina (Quintero et al., 2020). It has muscles that control the opening and closing of the pupil (Wang et al., 2017). Iris has many important features (Khalaf et al., 2018) in its structure, such as the crypt, collarette, corona, and freckle. These unique features are different for everyone (Pavaloi & Ignat, 2019) and remain stable (Vyas et al., 2019); thus, they are suitable for biometric recognition. Even cataract surgery does not alter iris features (Barpanda et al., 2019). However, iris features can minimally change over time (De Marsico et al., 2018), such as in people suffering from diabetes (Azimi et al., 2019).

Iris segmentation is a part of iris recognition where it separates the accurate iris boundary from additional noises (Arsalan et al., 2019). It is important and crucial because it can lay a good foundation for efficient iris recognition (Zhang et al., 2019). Moreover, iris segmentation can limit errors and maintain good accuracy (Wu & Zhao, 2019). The error generated in iris segmentation can be propagated to the other parts of iris recognition (Arsalan et al., 2018). An accurate iris recognition must have an accurate iris segmentation (Rapaka & Kumar, 2018).

There are many iris segmentation methods that have been published in recent years. Arsalan et al. (2017) deployed an iris segmentation in a noisy environment from the convolutional neural network. On the other hand, Proenca and Neves (2018) used the deep learning framework for periocular recognition without using any segmentation mask. Other than that, deep neural network can be used for iris segmentation (Bazrafkan et al., 2018; Zhao & Kumar, 2018). Meanwhile, the non-ideal iris images with non-uniform illumination and non-circular iris boundary can also be segmented (Jan, 2017). Various works achieved good performance when using the active contour approaches such as those reported in Ouabida et al. (2017), Chen et al. (2015), Jamaludin et al. (2018), Akinfende et al. (2020), and Jamaludin et al. (2017).

In a non-ideal environment, the iris boundary is normally oval and unsymmetrical. Still, the active contour can segment the precise iris region and obtain acceptable segmentation accuracy and recognition accuracy in this environment. Additionally, the iris region obstructed by reflection, eyelash, and eyelid can be located. Nevertheless, it is

currently unclear how active contour responds to blurry iris images or motion blur instead of various noises, which presents a significant obstacle in iris segmentation. The investigation of blurry iris images for initial contour is rarely published and must be clarified. Moreover, the evolution or convergence speed remains a significant challenge for active contour as it segments the precise iris boundary.

Experiments have been implemented in this study to achieve an efficient iris segmentation algorithm in terms of accuracy and fast execution, according to the aforementioned concerns. In addition, initial contour has been explored to define its position. To accomplish these goals, the morphological closing and Wiener filter have been deployed for pre-processing and reflection removal. Next, the adaptive initial contour (AIC), δ, and stopping function have been integrated to create the adaptive Chan-Vese active contour (ACVAC) algorithm. Finally, the partly-normalization method for normalization and feature extraction has been designed by selecting the most prominent features in the iris region. The limitation of this study is that the blurry iris images are simulated to produce the motion blur effect.

ACTIVE CONTOUR

Segmentation without Edges Model

Active contour models, namely snake, gradient vector flow (GVF), balloon, and geodesic active contour (GAC) can be used for image segmentation. These active contour models depend on edge detection for the segmentation process. Following this, Chan and Vese (2001) introduced a new active contour model to reduce dependency on edge detection. This model uses a two-phase constant model energy function to detect boundaries in images, instead of gradient information. It can segment various shapes of boundaries in noisy images that are not necessarily defined by edge or gradient. This method is also called segmentation without edges since it ignores edges in images.

The Chan-Vese (CV) active contour model is an approximation of the segmentation method with the level set method by Mumford and Shah (1989). The energy function $F(c_1,c_2,C)$ was minimized by segmenting an image into two elements, i.e., background and foreground. Then,

the curve evolved to reach the expected boundary. The energy function (Mumford & Shah, 1989) is shown in Equation 1:

$$F(c_1, c_2, C) = \mu \bullet Length(C) + v \bullet Area(inside(c)) + \lambda_1 \int_{inside(C)} |\mu_0(x,y) - c_1|^2 dxdy + \lambda_2 \int_{outside(c)} |\mu_0(x,y) - c_2|^2 dxdy \quad (1)$$

where c_1 is a constant of average μ_0 inside curve C, c_2 is a constant of average μ_0 outside curve C, μ is a length parameter or scaling role, μ_0 is an image, and constants λ_1, λ_2, and v. The first term of the formula represents the regularity of curve C. The second term controls the area of C. The third and fourth terms represent the discrepancy between c_1 and c_2.

Unfortunately, this active contour was susceptible to initialization. Since the energy function was non-convex, the initialization overloaded local minima (Chan & Vese, 2001). Moreover, the CV active contour showed good segmentation performance as in Ma et al. (2018) and Yu et al. (2018), whereby the medical images had stable and less complex textures. In spite of this, the iris has many rich features and complex structures such as furrows, crypts, and collarette. Crypts may be unusually dark with thick radial fibers (Chen et al., 2015; Shah & Ross, 2009). These factors can lead to active contour to activate the stopping function, thus not converging to the correct boundary.

Recent Models

Many active contour approaches for iris segmentation have recently been created to solve previous concerns. Chang et al. (2020) used the GAC model for iris region segmentation. To achieve the correct pupil center and radius, the GAC model was used to segment the pupil area. Then, the iris circle calculation was used for precise iris region segmentation. This method obtained a good performance of initial contour position and segmentation accuracy. The formula for iris circle detection (Chang et al., 2020) is shown in Equation 2:

$$K(x,y) = \frac{1}{1 + \left(\frac{\|\nabla(G(x,y) * I(x,y))\|}{k} \right)^{\alpha}} \quad (2)$$

where *I(x,y)* is an iris image, *G(x,y)* is an initial contour image, and α and *k* are constants.

However, this method used many pre-processing algorithms such as Gaussian filter, Hough transform (HT), and Canny edge detection (CED) for pupil segmentation, which can affect its computational speed. Furthermore, in non-ideal and blurry images, the initial contour was not adequate for the correct iris region segmentation.

On the other hand, Abdullah et al. (2016) deployed the GVF model for iris segmentation. In order to produce a fusion of shrinking and expanding active contours, a novel force was introduced to the GVF model. The failure detection of a non-convex object and initial curve sensitivity could be minimized by preventing the target contour from shrinking and disappearing if it lay inside of the curve. Based on the results, this method obtained good accuracy for non-ideal segmentation. Moreover, the initial contour position managed to segment the precise boundary. The formula for the GVF model (Abdullah et al., 2016) is shown in Equation 3:

$$\iint \mu(u_x^2 + u_y^2 + v_x^2 + v_y^2) + |\nabla f|^2 |V - \nabla f|^2 \, dxdy \tag{3}$$

where v_x, v_y, u_x and u_y are the partial derivatives of *v(x,y)* and *u(x,y)* in the *x* and *y* directions.

Nevertheless, this method also used the circular HT and CED for pupil segmentation and initialization. It utilized two active contours for the segmentation of the iris and pupil, which could further reduce its speed. In addition, the developed initial contour segmented the non-ideal iris images only.

On the other hand, the CV active contour model was used by Chen et al. (2015) for iris segmentation. This method employed the pixel gray information to develop the initial contour. The center of the iris region was obtained from the coarse localization of the pupil. The interference factors were evaluated to set the CV active contour parameter. The search range was limited between 180^0 to 210^0 and 330^0 to 360^0. The proposed method achieved good segmentation accuracy in the noisy images and non-ideal iris images such as Poisson and Gaussian noises. The curve evolution termination criterion managed

to stop the energy function in an appropriate boundary. The formula for CV active contour (Chen et al., 2015) is shown in Equation 4:

$$F(c_1, c_2, C) = \alpha \bullet \mu \bullet Length(C)_{+\ldots} \quad (4)$$

This method used the Gaussian filter and CED for pupil segmentation and initialization, which could increase its computational speed. Similar to Abdullah et al. (2016), Chen et al.'s (2015) method applied two active contours for iris and pupil segmentations, which could affect its speed. The developed initial contour position could segment the precise iris region with various noises, but the effect of motion blur was mentioned. Furthermore, the stopping function was not adequate for the blurry iris images, causing the curve to evolute and expand to the eyelash and eyelid.

THE PROPOSED ALGORITHM

Overview

The proposed adaptive Chan-Vese active contour (ACVAC) algorithm is based on the CV active contour model, as the original model is less reliant on edge detection. The algorithm will be deployed in the blurry iris images to locate the precise iris region. This work is divided into pre-processing, adaptive initial contour (AIC), partly-normalization, and performance analysis.

Pre-Processing

Blurry images occur due to image capturing disturbances such as object or camera movement, insufficient capture time, poor focus, and scattered light. Furthermore, this occurs regularly in an uncontrolled environment. As a result, pre-processing is required to enhance the quality of the image.

In this study, the Wiener filter approach was employed to increase the quality of iris images, as described in Jamaludin et al. (2021) and Baselice et al. (2018). For image deblurring, this method outperforms the Lucy-Richardson and blind deconvolution algorithms. The point spread function was set up by determining the blurry pixel width using the optical system light. Then, the Gaussian low-pass filter was

employed for applying the constraint of the point spread function (PSF). The Wiener filter mechanism can adapt to the motion blur environment described by the PSF; thus, it will be able to produce better iris textures. In addition, the image's key features can be preserved. The formula for the Wiener filter $W(f_1,f_2)$ is shown in Equation 5:

$$W(f_1,f_2)=\frac{H*(f_1,f_2)S_x(f_1,f_2)}{\left|H(f_1,f_2)\right|^2 S_x(f_1,f_2)+S_n(f_1,f_2)} \quad (5)$$

where $H(f_1,f_2)$ is the blurring filter, $S_x(f_1,f_2)$ is the original power spectra, and $S_n(f_1,f_2)$ is the noise power spectra (Baselice et al., 2018). The pre-processing example is shown in Figure 1.

Figure 1

Pre-Processing on Blurry Iris Image where a) Iris Image before Pre-Processing b) Iris Image after Pre-Processing

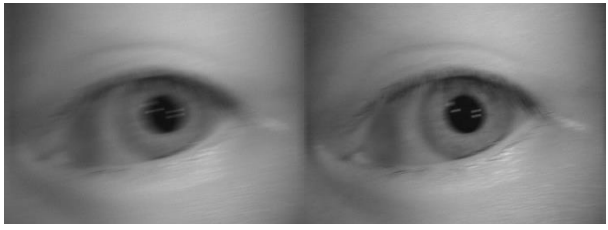

a) b)

AIC

Pre-processing can only minimally improve the blurry iris textures. As a result, AIC is developed in blurry iris images for precise iris region segmentation.

Firstly, in the discontiguous and contiguous regions, all pixel values were calculated to segment the pupil region. The specific pupil threshold was computed from the pre-test on 100 iris images. The information of the adaptable radius variable and convergence threshold was also investigated during the pre-test. Next, the connected components in the image were analyzed from the acquired data. Then, the connected

components were sorted to determine the specific location of the pupil region in the iris image. The biggest connected component in the image was the desired pupil region. The radius and centroid of the pupil region were also recorded. Sometimes, the eyelash region can be detected as an accurate pupil region. However, inaccurate detection can be prevented by the assigned pupil threshold.

The abovementioned method was also used to detect reflections in iris images. Furthermore, morphological closing was applied to remove the detected reflections. Firstly, complementation was employed to the iris image. The dark regions indicated reflections. All bright regions were enlarged and connected with morphological closing. The closest neighbors' pixels were filled into the dark regions, thus eliminating reflections.

Active contour for iris and pupil segmentations, which has been used by recent active contour-based algorithms (Chen et al., 2015; Chang et al., 2020; Abdullah et al., 2016), is a computational-hungry method. For this reason, the proposed algorithm created an initial contour from the previously obtained centroid and radius information. On the other hand, the prominent edges in an image can create inaccurate segmentation if approached by the evolution curve. The prominent edges with rich textures are typically observed at the upper eyelash, thus the curve expands to the eyelash and end abruptly. As a result, the initial contour should not be based exclusively on the pupil region centroid, as it may intercept with the eyelash (Jamaludin et al., 2018). In this study, the evolution curve could steer clear from the prominent edges, as the AIC was developed with the pupil centroid, and was relocated away from the upper eyelash. The proposed AIC is shown in Equation 6:

$$AIC = \varepsilon r_p - \sqrt{(x - x_P)^2 + (y - y_P + k)^2} \tag{6}$$

where ε is an adaptable radius variable, r_p is the pupil radius, x_p and y_p are the pupil centroid coordinates, and k is the relocated y-axis from the upper eyelash. εr_p creates a region-of-interest (ROI) from the AIC centroid, thus minimizing the search area.

The length parameter μ is a significant scaling factor that influences the length of the evolution curve. In order to avoid incorrect iris segmentation, this parameter must be adjusted appropriately. μ can

integrate the searched iris region when the evolution curve length is restrained. Previously in Chen et al. (2015), the interference evaluation factor was employed: large μ for large object segmentation such as pupil and iris, and small μ for small object segmentation such as eyelash. In this study, δ was developed from the upper eyelash to restrain the length of the evolution curve, where μ evolved toward the large object. The formula of δ is shown in Equation 7:

$$\delta = \frac{\omega}{(N_{AIC} + \varepsilon r_P) N_{AIC}} \tag{7}$$

where ω is the count number of pixel 0 in the upper eyelash region, and N_{AIC} is a square ROI based on AIC at the upper eyelash region. εr_p ensures interceptions between ROI and AIC, thus the length of evolution curve is restrained.

The evolution curve continues to expand until it reaches the correct iris boundary. False segmentation can happen if the eyelash interferes and stops the evolution curve at the inaccurate iris boundary. Therefore, the stopping function is developed, whereby the curve will stop if it approaches the iris boundary. Previously, two stopping functions were employed in Chen et al. (2015). In this study, one active contour was deployed by the modified stopping function. The modified stopping function is shown in Equations 8 and 9, where the evolution of curve starts from εr_p:

$$\inf_{c_1, c_2, C} \left\{ F^{ACVAC}(c_1, c_2, C) \right\} \approx \delta \bullet \mu \bullet Length(C) \tag{8}$$

$$Length(C) = \frac{\left| Length(C(t+1)) - Length(c(t)) \right|}{2} \tag{9}$$

If the defined convergence threshold is bigger than *Length (C)*, then the curve will stop evolving because of the stopping function. The previous pre-test determined the value of the convergence threshold.

Finally, the proposed AIC, δ, and stopping function were integrated into the ACVAC algorithm. The ACVAC algorithm F^{ACVAC} is shown in Equation 10:

$$F^{ACVAC}(c_1, c_2, C) = \delta \bullet \mu \bullet Length(C) + v \bullet Area(inside(c)) + \lambda_1 \int_{inside(C)} |\mu_0(x,y) - c_1|^2 \, dxdy + \lambda_2 \int_{outside(c)} |\mu_0(x,y) - c_2|^2 \, dxdy \quad (10)$$

where constants $\lambda_1 = \lambda_2 = 1$, $v \geq 0$, and iteration threshold = 25.

Partly-Normalization

Normalization is a process to convert iris features to the rectangular coordinate from the circular boundary. The same iris region can be referred to by the commonly used rubber sheet model, regardless of iris dilation or constriction (Jamaludin et al., 2018). Despite that, this method will collect all iris features including those that are not prominent enough for recognition, such as near the outer iris boundary (Abdullah et al., 2016). Therefore, this method is not efficient since the less important features are also included for feature extraction and normalization.

In this study, partly-normalization was created from the existing rubber sheet model. This model was refined where normalization was employed on the selected 70 percent iris region near the inner iris boundary (r = 0.7). Subsequently, the mapped iris feature points were reduced from normalization. The inner iris boundary had more prominent iris features than the outer iris boundary. Furthermore, iris features near the outer iris boundary could be obstructed by the upper eyelash. The proposed partly-normalization model is illustrated in Figure 2, where r = 0 – 1 represents the outer radius of the circular iris region, and θ = 0 – 360 represents the angular value of the circular iris region. Meanwhile, Figure 3 shows the iris features extracted by partly-normalization.

Figure 2

Partly-Normalization. The Red Box Represents 70 Percent of Iris Region Near to the Inner Iris Boundary. The Yellow Line Represents the Most Prominent Iris Features in Iris Region

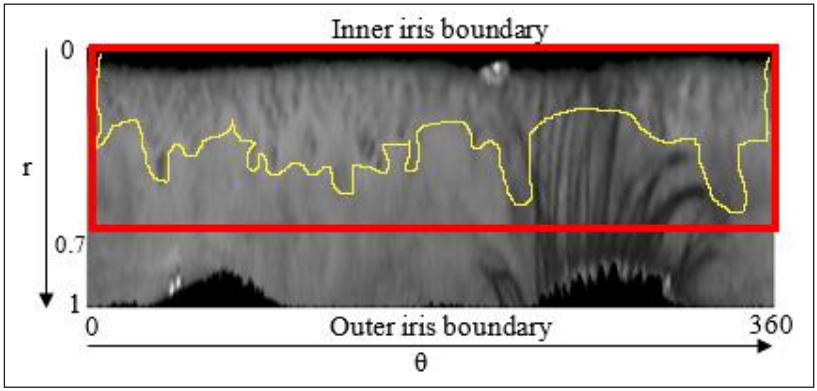

Figure 3

Iris Features Extracted by Partly-Normalization

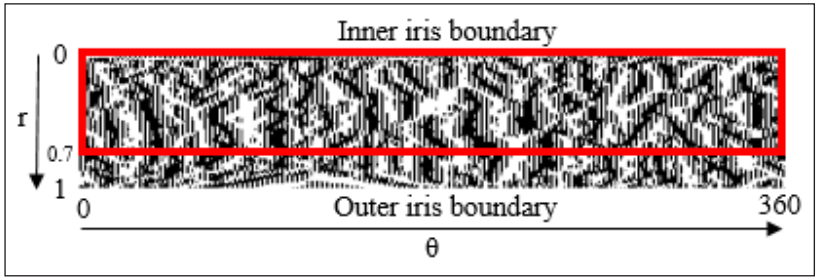

Finally, 1D Log-Gabor filter was employed for feature extraction as in Abdullah et al. (2016). The complete ACVAC algorithm is shown in Algorithm 1.

Algorithm 1: ACVAC	
1:	% Pre-processing
2:	PSF = fspecial('motion');
3:	A = image;
4:	Idouble = im2double(A);

(continued)

Algorithm 1: ACVAC

```
blurred = imfilter(Idouble,PSF,'conv','circular');
noise_mean = 0; noise_var = 0.0001;
blurred_noisy = imnoise(blurred, 'gaussian', noise_mean, noise_var);
estimated_nsr = noise_var / var(Idouble(:));
wnr1 = deconvwnr(blurred,PSF,estimated_nsr); % Wiener filter

% AIC
s=regionprops(A<threshold,'Area','PixelList');
areas=[s.Area].';
findAr=find(areas==max(areas));
ind=find(areas==areas(findAr));
pix=s(ind).PixelList;
full=sum(areas);
mask=logical(full(sparse(pix(:,2), pix(:,1), 1, size(A,1), size(A,2))));

% Active contour
ss=regionprops(mask,'Centroid','MajorAxisLength','MinorAxisLength');
diameters = mean([ss.MajorAxisLength ss.MinorAxisLength],2);
radii = diameters/2;
bww = activecontour(A, d,ItNu, 'chan-vese','SmoothFactor',SF,
'ContractionBias',CB);

% Feature extraction
nscales=1;minWaveLength=18;mult=1;
sigmaOnf=0.5;
[template,mask] = encode2
(image, noise, nscales, minWaveLength, mult, sigmaOnf);

% Partly-normalization
pn1 = image(1:(n*r),1:round(theta/2)); % iris code
pn2 = noise(1:(n*r),1:round(theta/2)); % noise mask

% Matching
hd = gethammingdistance2(pn1, mask1, pn2, mask2, 1);
```

Performance Analysis

The segmentation result must be evaluated to calculate the accuracy of the developed ACVAC algorithm. Segmentation accuracy was obtained by calculating the ratio of the segmented region over the

ground-truth region. The segmentation accuracy per image E_i is shown in Equation 11:

$$E_i = \frac{1}{m \times n} \sum_{x=1}^{m} \sum_{y=1}^{n} (S_{x,y} \otimes G_{x,y}) \quad (11)$$

where m and n are the height and width of iris image i, $S(x,y)$ is the segmented iris region, and $G(x,y)$ is the ground-truth iris region. Then, the overall segmentation accuracy E was computed by averaging E_i to the entire tested iris images N, as shown in Equation 12:

$$E = \frac{1}{N} \sum_{i=1}^{N} E_i \quad (12)$$

The highest percentage of the overall segmentation accuracy indicated the most accurate iris segmentation algorithm.

ANALYSIS AND RESULTS

Tools and Instruments

The pupil threshold, adaptable radius variable and convergence threshold were investigated from the pre-test of selected 100 iris images of the CASIA v4 database. After that, these parameters were averaged and updated into the proposed ACVAC algorithm. Next, 400 blurry iris images were experimented with the ACVAC algorithm. To create a motion blur environment, these iris images were blurred.

The proposed algorithm was developed and experimented on a computer. The computational environment for the experiment included the following criteria: Windows 8.1 Pro 64-bit, Intel i5-4690K 3.50 GHz, 16 GB RAM, and MATLAB 2020b. The performance of the proposed algorithm was compared with the other reported active contour-based algorithms. The reported segmentation algorithms were re-implemented with the same CASIA v4 database, and then the images were processed with the developed normalization and feature extraction methods.

AIC Deployment

The proposed model is sensitive to initialization, thus the precise position for initialization is placed at the correct boundary (Duan et

al., 2020). The segmentation accuracy and convergence time can be affected if its position is inaccurate. Figure 4 illustrates the precise initial contour position.

Figure 4

The Selected Results of AIC Where the White-Red Circles are the Proposed AIC, the Red Boxes are the Square ROI, the Green Regions are the Intercepted Region, and the Plus Signs are the Pupil Centroid

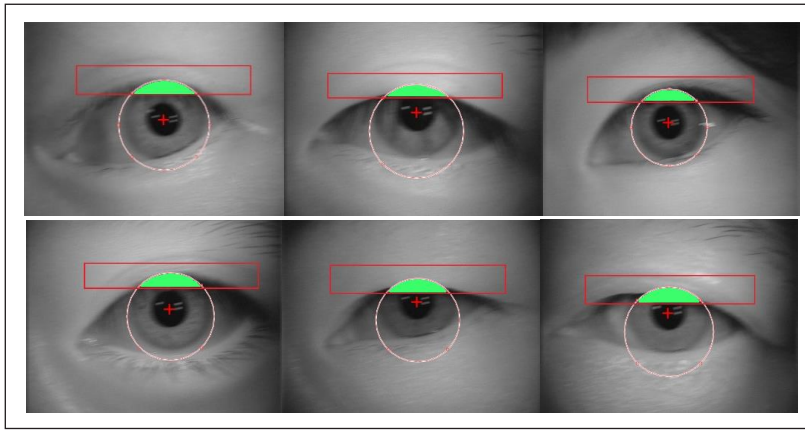

The designed AIC as shown in Figure 4 was created from the centroid of the pupil. AIC had a similar value to the x-axis value of the pupil region. In addition, the value of the y-axis was designed in a way where it would steer away from the upper eyelash region. As a result, just a fraction of the prominent edges with rich textures in the upper eyelid region was covered by the AIC. Furthermore, the AIC centroid was used to create the square ROI. The intercepted region of the square ROI and AIC was prohibited from the segmentation. The curve evolved and explored the lower eyelid region for the correct iris boundary until the intercepted region was reached. Finally, the curve stopped abruptly after reaching the upper eyelid and eyelash. As the rich energy levels and edges were avoided, the precise initial contour was obtained, which was in line with the findings of Jamaludin et al. (2018).

Iris Segmentation on Blurry Iris Images

Segmentation accuracy is the best indicator to analyze the performance of the iris segmentation algorithm. Therefore, Figure 5 demonstrates

the selected blurry iris images with the proposed segmentation algorithm.

Figure 5

The Selected ACVAC Segmentation Results

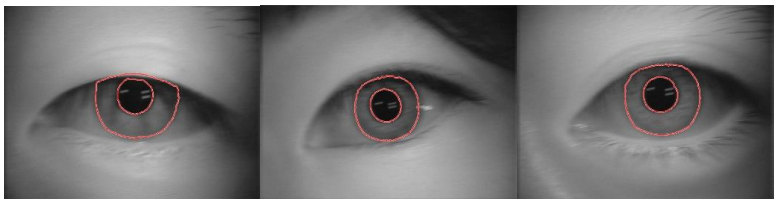

a) Segmentation on blurry and heavy eyelash occlusions

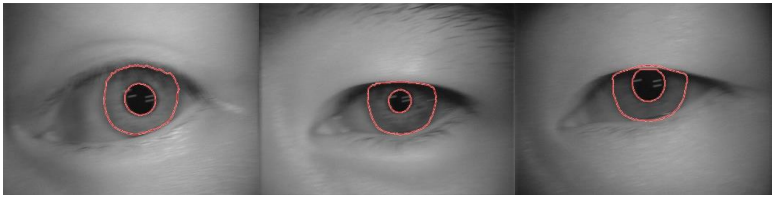

b) Segmentation on blurry and heavy eyelid occlusions

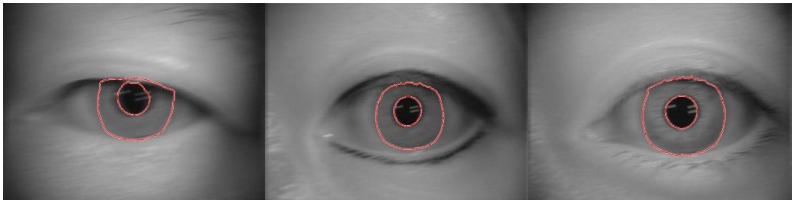

c) Segmentation on double eyelids occlusions

The employed ACVAC algorithm in the blurry iris images could segment the precise iris boundaries as illustrated in Figure 5. Meanwhile, the segmentation results for the blurry and heavy eyelash occlusions are shown in Figure 5(a). In addition, the segmentation results on the blurry and heavy eyelid occlusions can be observed in Figure 5(b). Moreover, Figure 5(c) shows the segmentation results of the double eyelids occlusions. The abovementioned figures proved that the proposed algorithm with AIC, δ, and stopping function could

correctly identify the sclera, pupil, lower, and upper eyelids. As stated in the previous section, the position of AIC was accurate in the blurry images. Moreover, the search area excluded the pupil region and upper eyelash, thus allowing δ to restrain the length of the curve. Meanwhile, the search area included the lower eyelid, which had a small amount of rich textures. Moreover, when the convergence threshold was bigger than *Length (C)*, the stopping function halted the curve after it reached the precise iris region. Due to the aforementioned factors, a separate eyelid detection was not required. The non-ideal and noisy iris segmentation accuracy was increased from the abovementioned parameters, which was in line with the study reported in Abdullah et al. (2016). Nevertheless, the previous study (Abdullah et al., 2016) did not deploy its algorithm on blurry images.

Furthermore, the proposed algorithm achieved a higher average segmentation accuracy than prior active contour-based approaches, as presented in Table 1.

Table 1

Average Segmentation Accuracy and Average Computational Time Comparison

Method	Average Segmentation Accuracy (%)	Average Computational Time (s)
Chen et al. (2015)	81.2	1.81
Jamaludin et al. (2018)	48.6	0.71
Chang et al. (2020)	76.1	1.90
Abdullah et al. (2016)	77.6	2.31
Proposed method	97.2	0.65

The segmentation accuracy of 97.2 percent was achieved by the proposed method. The one that came closest was the method used by Chen et al. (2015), which obtained a segmentation accuracy of 81.2 percent. Several factors were discussed based on the aforementioned segmentation accuracy results. Pixel gray information was used to design the initial contour in Chen et al. (2015). Satisfactory segmentation accuracy was obtained on the noisy and non-ideal iris images. Despite that, the less precise position of initial contour for the detection of the blurry upper eyelid boundary on the blurry iris

images gave an unsatisfactory result. Moreover, the curve expansion along the upper eyelash and eyelid was insufficient for the stopping function. Meanwhile, the CV active contour was used in Jamaludin et al.'s (2018) method for iris segmentation. The iris radius was assumed to be three times the size of the pupil radius for the development of the initial contour position. It emphasized the lower iris region, thus obtaining the lowest segmentation accuracy. Meanwhile, HT, CED, and GAC were used in Chang et al. (2020) to create the initial contour position. Non-ideal images could be segmented with this approach. However, it could mislead the iris circle estimation as it located the hidden circles in the images. On the other hand, GVF active contour was utilized in Abdullah et al. (2016) for iris segmentation. Here, the non-convex object detection failure and initial curve sensitivity were used to optimize the position of the initial contour. However, this position was only precise for non-ideal iris segmentation.

A few factors have been identified that allow the proposed algorithm to obtain the highest segmentation accuracy on blurry images. Firstly, the proposed ACVAC algorithm was designed from AIC that allowed for accurate initialization. The segmentation accuracy increased with accurate initialization, which was in line with Ding et al. (2017). Secondly, the efficient convergence mechanism was created where the designed δ restrained the evolution curve length. This finding was consistent with Jin and Weng (2019), whereby the smooth boundary could be obtained if the curve length was controlled. Thirdly, the curve stopped evolving when it approached the precise iris boundary by using the modified stopping function.

Computational Time

Computational time is the best indicator to evaluate how fast the algorithm can be executed. Table 1 demonstrates that the proposed method outperformed the other active contour-based methods. The method required fewer operations in its design. For iris segmentation, it used a Wiener filter, morphological closing, and one active contour. In addition, the position of the initial contour aided in the computational speed. Iteration for boundary convergence could also be reduced if the initial contour position was accurate. This was in line with Fang et al. (2019), which stated that the execution time for iris segmentation could be reduced if the active contour had a small iteration. Furthermore, the partly-normalization method minimized the mapped

points from the segmented region, thus reducing computational time when processing the blurry iris images. The algorithm's performance could be improved if it had fewer processes for normalization, which was in line with Jamaludin et al. (2018).

Furthermore, the circle detection methods, namely HT and integro-differential operator, are computational-consuming processes (Djekoune et al., 2017). The proposed algorithm was faster than the other methods since the circle detection algorithm was not used. The slow computational time in Chang et al. (2020) could be attributed to the Gaussian filter, CED, and HT used for the coarse pupil region. Meanwhile, Abdullah et al. (2016) applied CED and circular HT for initialization before active contour was implemented. This method used two active contours, which further reduced its computational speed. Meanwhile, the circle detection algorithm was not utilized in Chen et al. (2015). Nevertheless, two active contours required more computational time for segmentation. In addition, the previous study (Chen et al., 2015) used the Gaussian filter and Canny edge detection for initialization. The method in Jamaludin et al. (2018) segmented the sub-iris region, thus achieving an almost similar computational time as the proposed algorithm. For pre-processing, it used the flood-fill and morphological closing operations. Meanwhile, iris segmentation used only one active contour.

CONCLUSION

In this study, the ACVAC algorithm was proposed for blurry iris image segmentation. This algorithm was based on AIC and partly-normalization. The proposed algorithm comprised pre-processing, AIC, and partly-normalization methods. For pre-processing, the blurry iris images were deblurred and reflections were eliminated with the Wiener filter and morphological closing. Then, the segmentation accuracy was improved by designing AIC, δ, and stopping function. Only a small amount of prominent edges was covered by the designed AIC. Furthermore, the curve's length was restrained by employing δ. Finally, the partly-normalization method was employed for feature extraction and normalization, where the most prominent iris features were selected.

The obtained results showed that the proposed algorithm achieved the highest segmentation accuracy and fastest computational time

than the other active contour-based methods. The accurate position of the initial contour on the blurry iris images was clearly defined. The convergence speed was enhanced by employing fewer pre-processing, minimum active contour, and partly-normalization. Therefore, this study clarified that active contour can segment blurry iris images if an accurate initial contour can be produced. This can also increase the recognition accuracy for blurry iris image segmentation. For future research, the proposed algorithm can be refined with a graphic processing unit (GPU) to reduce the high computational cost of active contour.

ACKNOWLEDGMENT

This research received no specific grant from any funding agency in the public, commercial, or not-for-profit sectors. The authors would like to thank the Chinese Academy of Sciences' Institute of Automation (CASIA) for the CASIA v4 database.

REFERENCES

Abdullah, M. A., Dlay, S. S., Woo, W. L., & Chambers, J. A. (2016). Robust iris segmentation method based on a new active contour force with a noncircular normalization. *IEEE Transactions on Systems, Man, and Cybernetics: Systems*, *47*(12), 3128–3141. https://doi.org/10.1109/TSMC.2016.2562500

Akinfende, A. S., Imoize, A. L., & Ajose, S. O. (2020). Investigation of iris segmentation techniques using active contours for non-cooperative iris recognition. *Indonesian Journal of Electrical Engineering and Computer Science*, *19*(3), 1275–1286. https://doi.org/10.11591/ijeecs.v19.i3.pp1275-1286

Alsmirat, M. A., Al-Alem, F., Al-Ayyoub, M., Jararweh, Y., & Gupta, B. (2019). Impact of digital fingerprint image quality on the fingerprint recognition accuracy. *Multimedia Tools and Applications*, *78*(3), 3649–3688. https://doi.org/10.1007/s11042-017-5537-5

Amreen, S., Mockus, A., Zaretzki, R., Bogart, C., & Zhang, Y. (2020). ALFAA: Active learning fingerprint based anti-aliasing for correcting developer identity errors in version control systems. *Empirical Software Engineering*, *25*(2), 1136–1167. https://doi.org/10.1007/s10664-019-09786-7

Anne, N., Dunbar, M. D., Abuna, F., Simpson, P., Macharia, P., Betz, B., & Carey, F. (2020). Feasibility and acceptability of an iris biometric system for unique patient identification in routine HIV services in Kenya. *International Journal of Medical Informatics*, *133*, 104006. https://doi.org/10.1016/j.ijmedinf.2019.104006

Arsalan, M., Hong, H. G., Naqvi, R. A., Lee, M. B., Kim, M. C., Kim, D. S., Kim, C. S., & Park, K. R. (2017). Deep learning-based iris segmentation for iris recognition in visible light environment. *Symmetry*, *9*(11), 263. https://doi.org/10.3390/sym9110263

Arsalan, M., Kim, D. S., Lee, M. B., Owais, M., & Park, K. R. (2019). FRED-Net: Fully residual encoder–decoder network for accurate iris segmentation. *Expert Systems with Applications*, *122*, 217–241. https://doi.org/10.1016/j.eswa.2019.01.010

Arsalan, M., Naqvi, R. A., Kim, D. S., Nguyen, P. H., Owais, M., & Park, K. R. (2018). IrisDenseNet: Robust iris segmentation using densely connected fully convolutional networks in the images by visible light and near-infrared light camera sensors. *Sensors*, *18*(5), 1501. https://doi.org/10.3390/s18051501

Azimi, M., Rasoulinejad, S. A., & Pacut, A. (2019). Iris recognition under the influence of diabetes. *Biomedical Engineering/Biomedizinische Technik*, *64*(6), 683–689. https://doi.org/10.1515/bmt-2018-0190

Barpanda, S. S., Majhi, B., Sa, P. K., Sangaiah, A. K., & Bakshi, S. (2019). Iris feature extraction through wavelet mel-frequency cepstrum coefficients. *Optics and Laser Technology*, *110*, 13–23. https://doi.org/10.1016/j.optlastec.2018.03.002

Baselice, F., Ferraioli, G., Ambrosanio, M., Pascazio, V., & Schirinzi, G. (2018). Enhanced wiener filter for ultrasound image restoration. *Computer Methods and Programs in Biomedicine*, *153*, 71–81. https://doi.org/10.1016/j.cmpb.2017.10.006

Bazrafkan, S., Thavalengal, S., & Corcoran, P. (2018). An end to end deep neural network for iris segmentation in unconstrained scenarios. *Neural Networks*, *106*, 79–95. https://doi.org/10.1016/j.neunet.2018.06.011

Blasco, J., & Peris-Lopez, P. (2018). On the feasibility of low-cost wearable sensors for multi-modal biometric verification. *Sensors*, *18*(9), 2782. https://doi.org/10.3390/s18092782

Chan, T. F., & Vese, L. A. (2001). Active contours without edges. *IEEE Transactions on Image Processing*, *10*(2), 266–277. https://doi.org/10.1109/83.902291

Chang, Y. T., Shih, T. K., Li, Y. H., & Kumara, W. G. C. W. (2020). Effectiveness evaluation of iris segmentation by using geodesic active contour (GAC). *The Journal of Supercomputing*, *76*(3), 1628–1641. https://doi.org/10.1007/s11227-018-2450-2

Chen, Y., Liu, Y., & Zhu, X. (2015). Robust iris segmentation algorithm based on self-adaptive Chan-Vese level set model. *Journal of Electronic Imaging*, *24*(4), 043012. https://doi.org/10.1117/1.JEI.24.4.043012

Chen, Y., Wu, C., & Wang, Y. (2020). T-center: A novel feature extraction approach towards large-scale iris recognition. *IEEE Access*, *8*, 32365–32375. https://doi.org/10.1109ACCESS.2020.2973433

Cohen, F., Sowmithran, S., & Li, C. (2021). 3D iris model and reader for iris identification. *Concurrency and Computation: Practice and Experience*, *33*(12), e5653. https://doi.org/10.1002/cpe.5653

De Marsico, M., Nappi, M., Narducci, F., & Proenca, H. (2018). Insights into the results of miche i-mobile iris challenge evaluation. *Pattern Recognition*, *74*, 286–304. https://doi.org/10.1016/j.patcog.2017.08.028

Ding, K., Xiao, L., & Weng, G. (2017). Active contours driven by region-scalable fitting and optimized Laplacian of Gaussian energy for image segmentation. *Signal Processing*, *134*, 224–233. https://doi.org/10.1016/j.sigpro.2016.12.021

Djekoune, A. O., Messaoudi, K., & Amara, K. (2017). Incremental circle Hough transform: An improved method for circle detection. *Optik*, *133*, 17–31. https://doi.org/10.1016/j.ijleo.2016.12.064

Duan, Y., Peng, T., & Qi, X. (2020). Active contour model based on LIF model and optimal DoG operator energy for image segmentation. *Optik*, *202*, 163667. https://doi.org/10.1016/j.ijleo.2019.163667

Fang, J., Liu, H., Zhang, L., Liu, J., & Liu, H. (2019). Active contour driven by weighted hybrid signed pressure force for image segmentation. *IEEE Access*, *7*, 97492–97504. https://doi.org/10.1109/ACCESS.2019.2929659

Hossain, M. S., Balagani, K. S., & Phoha, V. V. (2021). Effectiveness of symmetric rejection for a secure and user convenient multistage

biometric system. *Pattern Analysis and Applications*, *24*(1), 49–60. https://doi.org/10.1007/s10044-020-00899-0

Jamaludin, S., Zainal, N., & Zaki, W. M. D. W. (2017). GPU implementation of sub-iris technique in iris recognition system. *Pertanika Journal of Science and Technology*, *25*(S)3, 263–274.

Jamaludin S., Zainal N., & Zaki W. M. D. W. (2016). Iris recognition based on the modified Chan-Vese active contour. *Jurnal Teknologi*, *78*(10–3), 13–17. https://doi.org/10.11113/jt.v78.9756

Jamaludin, S., Zainal, N., & Zaki, W. M. D. W. (2021). Deblurring of noisy iris images in iris recognition. *Bulletin of Electrical Engineering and Informatics*, *10*(1), 156–159. https://doi.org/10.11591/eei.v10i1.2467

Jan, F. (2017). Segmentation and localization schemes for non-ideal iris biometric systems. *Signal Processing*, *133*, 192–212. https://doi.org/10.1016/j.sigpro.2016.11.007

Jin, R., & Weng, G. (2019). A robust active contour model driven by fuzzy c-means energy for fast image segmentation. *Digital Signal Processing*, *90*, 100–109. https://doi.org/10.1016/j.dsp.2019.04.004

Kaur, B. (2020). Iris spoofing detection using discrete orthogonal moments. *Multimedia Tools and Applications*, *79*(9), 6623–6647. https://doi.org/10.1007/s11042-019-08281-x

Khalaf, E. T., Mohammad, M. N., & Moorthy, K. (2018). Robust partitioning and indexing for iris biometric database based on local features. *IET Biometrics*, *7*(6), 589–597. https://doi.org/10.1049/iet-bmt.2017.0130

Ma, C., Luo, G., & Wang, K. (2018). Concatenated and connected random forests with multiscale patch driven active contour model for automated brain tumor segmentation of MR images. *IEEE Transactions on Medical Imaging*, *37*(8), 1943–1954. https://doi.org/10.1109/TMI.2018.2805821

Mumford, D., & Shah, J. (1989). Optimal approximations by piecewise smooth functions and associated variational problems. *Communications on Pure and Applied Mathematics*, *42*(5), 577–685.

Ouabida, E., Essadique, A., & Bouzid, A. (2017). Vander Lugt correlator based active contours for iris segmentation and tracking. *Expert Systems with Applications*, *71*, 383–395. https://doi.org/10.1016/j.eswa.2016.12.001

Pavaloi, I., & Ignat, A. (2019). Iris image classification using SIFT features. *Procedia Computer Science*, *159*, 241–250. https://doi.org/10.1016/j.procs.2019.09.179

Proenca, H., & Neves, J. C. (2018). Deep-PRWIS: Periocular recognition without the iris and sclera using deep learning frameworks. *IEEE Transactions on Information Forensics and Security*, *13*(4), 888–896. https://doi.org/10.1109/TIFS.2017.2771230

Quintero, A. V., Perez-Merino, P., & De Smet, H. (2020). Artificial iris performance for smart contact lens vision correction applications. *Scientific Reports*, *10*(1), 1–12. https://doi.org/10.1038/s41598-020-71376-1

Rapaka, S., & Kumar, P. R. (2018). Efficient approach for non-ideal iris segmentation using improved particle swarm optimisation-based multilevel thresholding and geodesic active contours. *IET Image Processing*, *12*(10), 1721–1729. https://doi.org/10.1049/iet-ipr.2016.0917

Sarier, N. D. (2021). Comments on biometric-based non-transferable credentials and their application in blockchain-based identity management. *Computers and Security*, *105*, 102243. https://doi.org/10.1016/j.cose.2021.102243

Shah, S., & Ross, A. (2009). Iris segmentation using geodesic active contours. *IEEE Transactions on Information Forensics and Security*, *4*(4), 824–836. https://doi.org/10.1109/TIFS.2009.2033225

Shin, J., Kim, T., Lee, B., & Yang, S. (2017). IRIS-HiSA: Highly scalable and available carrier-grade SDN controller cluster. *Mobile Networks and Applications*, *22*(5), 894–905. https://doi.org/10.1007/s11036-017-0853-6

Shrivastava, H., & Tcheslavski, G. V. (2018). On the potential of EEG for biometrics: Combining power spectral density with a statistical test. *International Journal of Biometrics*, *10*(1), 52–64. https://dx.doi.org/10.1504/IJBM.2018.090128

Sujatha, E., & Chilambuchelvan, A. (2018). Multimodal biometric authentication algorithm using iris, palm print, face and signature with encoded dwt. *Wireless Personal Communications*, *99*(1), 23–34. https://doi.org/10.1007/s11277-017-5034-1

Vyas, R., Kanumuri, T., Sheoran, G., & Dubey, P. (2019). Efficient iris recognition through curvelet transform and polynomial fitting. *Optik*, *185*, 859–867. https://doi.org/10.1016/j.ijleo.2019.04.015

Wang, K., & Kumar, A. (2019). Cross-spectral iris recognition using CNN and supervised discrete hashing. *Pattern Recognition*, *86*, 85–98. https://doi.org/10.1016/j.patcog.2018.08.010

Wang, Q., Yue, W. W. S., Jiang, Z., Xue, T., Kang, S. H., Bergles, D. E., Mikoshiba, K., Offermanns, S., & Yau, K. W. (2017). Synergistic signaling by light and acetylcholine in mouse iris sphincter muscle. *Current Biology*, *27*(12), 1791–1800. https://doi.org/10.1016/j.cub.2017.05.022

Wu, X., & Zhao, L. (2019). Study on iris segmentation algorithm based on dense U-Net. *IEEE Access*, *7*, 123959–123968. https://doi.org/10.1109/ACCESS.2019.2938809

Yu, H., He, F., Pan, Y. (2018). A novel region-based active contour model via local patch similarity measure for image segmentation. *Multimedia Tools and Applications*, *77*(18), 24097–24119. https://doi.org/10.1007/s11042-018-5697-y

Zhang, M., He, Z., Zhang, H., Tan, T., & Sun, Z. (2019). Toward practical remote iris recognition: A boosting based framework. *Neurocomputing*, *330*, 238–252. https://doi.org/10.1016/j.neucom.2017.12.053

Zhang, W., Lu, X., Gu, Y., Liu, Y., Meng, X., & Li, J. (2019). A robust iris segmentation scheme based on improved u-net. *IEEE Access*, *7*, 85082–85089. https://doi.org/10.1109/ACCESS.2019.2924464

Zhao, Z., & Kumar, A. (2018). Improving periocular recognition by explicit attention to critical regions in deep neural network. *IEEE Transactions on Information Forensics and Security*, *13*(12), 2937–2952. https://doi.org/10.1109/TIFS.2018.2833018